Materials Science & Engineering A 596 (2014) 170–175

Contents lists available at ScienceDirect

Materials Science & Engineering A

journal homepage: www.elsevier.com/locate/msea

Indentation creep study on ultrafine-grained Zn processed by powder metallurgy

P. Jenei [a], J. Gubicza [a,*], G. Dirras [b], J.L. Lábár [a,c], D. Tingaud [b]

[a] Department of Materials Physics, Eötvös Loránd University Budapest, P.O.B. 32, H-1518, Hungary
[b] Université Paris 13, Sorbonne Paris Cité, Laboratoire des Sciences, des Procédés et des Matériaux, 99, avenue Jean Baptiste Clément, 93430 Villetaneuse, France
[c] Institute for Technical Physics and Materials Science, Research Centre for Natural Sciences, Hungarian Academy of Sciences, Budapest, Hungary

ARTICLE INFO

Article history:
Received 25 September 2013
Received in revised form
14 December 2013
Accepted 15 December 2013
Available online 22 December 2013

Keywords:
Nanostructured materials
Powder metallurgy
Indentation
Creep
Dislocations

ABSTRACT

Ultrafine-grained Zn (UFG-Zn) with the grain size of about 200 nm was processed by Spark Plasma Sintering at 300 °C from fine Zn powder. The grain boundaries in the consolidated material were decorated by ZnO dispersoids with a mean thickness of ~20 nm. The creep behavior was studied by indentation tests in the homologous temperature range of 0.87–0.91. The activation energy of the creep for UFG-Zn was found to be much larger (211–252 kJ/mol depending on the oxide content) than the value determined previously for coarse-grained Zn (152–159 kJ/mol). The activation energy increased with increasing ZnO content in UFG-Zn. X-ray line profile analysis revealed that the population of the different dislocation slip systems changed during creep deformation, indicating a considerable dislocation activity.

1. Introduction

The deformation mechanisms in hexagonal close-packed (hcp) metals depend strongly on the c/a ratio. In the case of hcp metals for which c/a is lower than 1.63 (e.g., in Ti or Zr), the dislocation slip is most easy in the prismatic plane while very large lattice resistance should be overcome in basal and pyramidal planes at low homologous temperatures and strain rates [1]. In metals with c/a ratio larger than 1.63 (such as Zn or Mg), the slip is most easy in the basal plane and the lattice resistance against dislocation glide is larger in the prismatic and pyramidal planes [1]. Additionally, twinning as a complementary deformation mechanism also plays an important role in the plasticity of hcp metals. With increasing temperature the lattice resistance in the non-easy slip planes decreases.

The high temperature deformation mechanisms in hcp metals with large c/a ratio can be easily studied on Zn due to its very low melting point (T_m=420 °C). Previous studies [2,3] have shown that although in the temperature range of 0.5–0.6 × T_m the activation energy is close to the value characteristic for self-diffusion (92 kJ/mole [1]), above 0.8 × T_m the creep of pure Zn can be characterized by anomalously high activation energy. Flinn and Munson [3] reported that above 270 °C the activation energy for the creep is about 152 kJ/mole. Tegart and Sherby [2] obtained 159 kJ/mole above 350 °C. The much higher activation energy as compared to self diffusion is generally explained by the rapid drop in the resistance to shear on non-basal systems with increasing temperature [1–3]. In addition, above 270 °C dynamic recrystallization is also suggested to contribute to the rapid increase of strain rate when the temperature is raised, resulting in higher apparent activation energy [4].

The observations summarized in the previous paragraph were obtained on coarse-grained pure Zn. However, the reduction of the grain size into the ultrafine or nanosized regime may change the main deformation mechanisms, thereby altering the characteristic parameters (e.g., the activation energy) of deformation and yielding extraordinary properties compared to the coarse-grained counterparts. The mechanical properties of ultrafine-grained (UFG) zinc in a wide range of strain rate and at near room temperature [5–7] have been investigated, but the high-temperature creep properties are missing from the literature. This can be explained by the low thermal stability of the UFG structure at high temperatures which results in recovery and recrystallization during the creep test. However, impurities and/or oxide dispersoids, which are usually unavoidable in powder metallurgy, can stabilize the microstructure [8].

In this paper, the high-temperature creep behavior of UFG-Zn is studied by indentation technique. Indentation tests can be effectively used to study the mechanical properties of materials [9–12] since this method is technically simpler than the tensile test. For instance, the sample preparation is easier and only a small amount of material is necessary for the investigations. This fact is extremely

* Corresponding author. Tel.: +36 1 372 2876; fax: +36 1 372 2811.
E-mail addresses: gubicza@metal.elte.hu, jeno.gubicza@gmail.com (J. Gubicza).

0921-5093/$ - see front matter © 2013 Elsevier B.V. All rights reserved.
http://dx.doi.org/10.1016/j.msea.2013.12.050

advantageous for UFG materials, where usually only small specimens are available. In the present investigations the UFG-Zn microstructure is obtained by the consolidation of fine powder particles, which process yields the formation of ZnO dispersoids at the Zn grain boundaries, stabilizing the grain structure in the creep experiments. From the activation energy and the change of the microstructure the underlying deformation mechanisms are determined. According to the knowledge of the authors, the study of the high temperature creep for UFG-Zn is missing from the literature.

2. Experimentals

2.1. Sample preparation

A UFG-Zn sample was processed by Spark Plasma Sintering (SPS) from a pure Zn powder with a fine average particle size of 150 nm supplied by UMICORE, Belgium. The dwell time, the applied pressure and the temperature of the SPS procedure were 5 min, 125 MPa and 300 °C, respectively. The phase composition of the as-consolidated material was characterized by X-ray diffraction using a Philips Xpert powder diffractometer with CuKα radiation (the wavelength is 0.15418 nm).

2.2. Characterization of the microstructure

The microstructure in the as-processed and the indented specimens was studied by electron backscattered diffraction (EBSD) and X-ray diffraction line profile analysis (XLPA). The EBSD investigation was carried out by a Zeiss Supra 40VP FEG scanning electron microscope. The step size between the neighboring measurement positions was 50 nm. The samples for EBSD investigations were prepared by mechanical grinding using 4000 grit SiC papers and a finish step using OP-S suspension from Struers. The total duration of the polishing process was about 20 min. The average grain size and the misorientation distribution of grain boundaries were extracted from the EBSD scans using an orientation imaging software OIM version 4 from TexSem Laboratories.

The X-ray line profiles were measured by a rotating anode diffractometer (Nonius, FR591) using CuKα_1 radiation (the wavelength is 0.15406 nm). Two-dimensional imaging plates were used for the detection of the Debye–Scherrer diffraction rings. The line profiles were determined as the intensity distribution perpendicular to the rings obtained by integrating the two-dimensional intensity distribution along the rings. The nineteen reflections in the diffraction angle range between 35° and 140° were evaluated by the Convolutional Multiple Whole Profile (CMWP) fitting analysis [13,14]. In this method, the experimental diffraction profiles are fitted by the convolution of the instrumental peaks and the theoretical line profiles related to the crystallite size, dislocations and twin faults. The CMWP procedure gives the crystallite size, the dislocation density, the parameters q_1 and q_2 depending on the prevailing dislocation slip systems and the twin boundary frequency. The latter quantity is defined as the relative fraction of twin boundaries among the lattice planes along their normal vector. The parameters q_1 and q_2 depend on the character of dislocations and therefore enable the determination of the prevailing dislocation slip systems in the specimen. The detailed description of the evaluation procedure of the slip systems from q_1 and q_2 is given in reference [15]. In this process the experimentally determined parameters q_1 and q_2 are compared to their theoretical values determined for the eleven possible slip systems in Zn [16,17]. These slip systems can be classified into three groups based on their Burgers vectors: $b_1=1/3\langle\bar{2}110\rangle$ ($\langle$a$\rangle$-type), $b_2=\langle 0001\rangle$ ($\langle$c$\rangle$-type) and $b_3=1/3\langle\bar{2}113\rangle$ ($\langle$c+a$\rangle$-type). Finally, the evaluation method gives the fractions of $\langle$a$\rangle$, $\langle$c$\rangle$ and $\langle$c+a$\rangle$ Burgers vector groups.

The microstructure of the samples was investigated by a JEOL 3010 transmission electron microscope (TEM) operated at 300 kV. The location and the morphology of ZnO in the Zn matrix were determined by energy-filtered TEM (EFTEM).

2.3. Indentation creep

The creep behavior was studied by indentation test using a home-made device in the temperature range of 330–360 °C. The indentation measurements were carried out by using a cylindrical punch with the diameter of 1.26 mm under constant load. The accuracy of the measured values of the displacement and the temperature were 50 nm and 1 °C, respectively. The impression velocity, v_i, and the applied force, F, were converted into equivalent tensile stress (σ) and strain rate ($\dot{\varepsilon}$), respectively, using the following formulas [10]:

$$\sigma = k_1 \frac{4F}{\pi d^2} \tag{1}$$

and

$$\dot{\varepsilon} = k_2 \frac{v_i}{d}, \tag{2}$$

where d is the diameter of the punch. k_1 and k_2 are constants with the values of 0.33 and 1, respectively.

3. Results

3.1. Microstructure of the as-consolidated material

X-ray diffraction analysis revealed the presence of ZnO phase (PDF: 36–1451) besides the hcp Zn matrix in the as-consolidated UFG-Zn sample (see Fig. 1). The ZnO phase was most probably formed from the native oxide layer on the surface of the fine powder particles. This layer was developed during powder processing before consolidation since the capsule containing the powder was broken in air and transferred to the graphite mold used as a sample holder during SPS. The ZnO content was characterized by the ratio of the integrated intensities for the Zn and ZnO peaks in the powder diffractogram obtained after background subtraction. This intensity ratio was 0.14 ± 0.01, indicating a high oxide content. In order to investigate the effect of ZnO content on the creep properties, another UFG-Zn material with much lower oxide fraction was processed from the same initial powder. In this procedure the capsule containing the powder was broken in Ar atmosphere instead of air and transferred to the graphite mold. This processing way yielded a much lower ZnO content characterized by the peak intensity ratio of 0.04 ± 0.01 (see Fig. 1). Hereafter, the materials

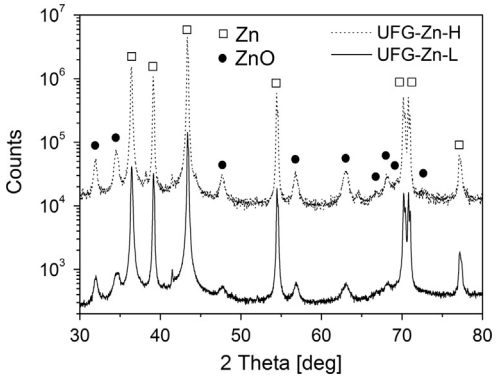

Fig. 1. X-ray diffractograms for UFG-Zn samples with high (UFG-Zn-H) and low (UFG-Zn-L) ZnO content.

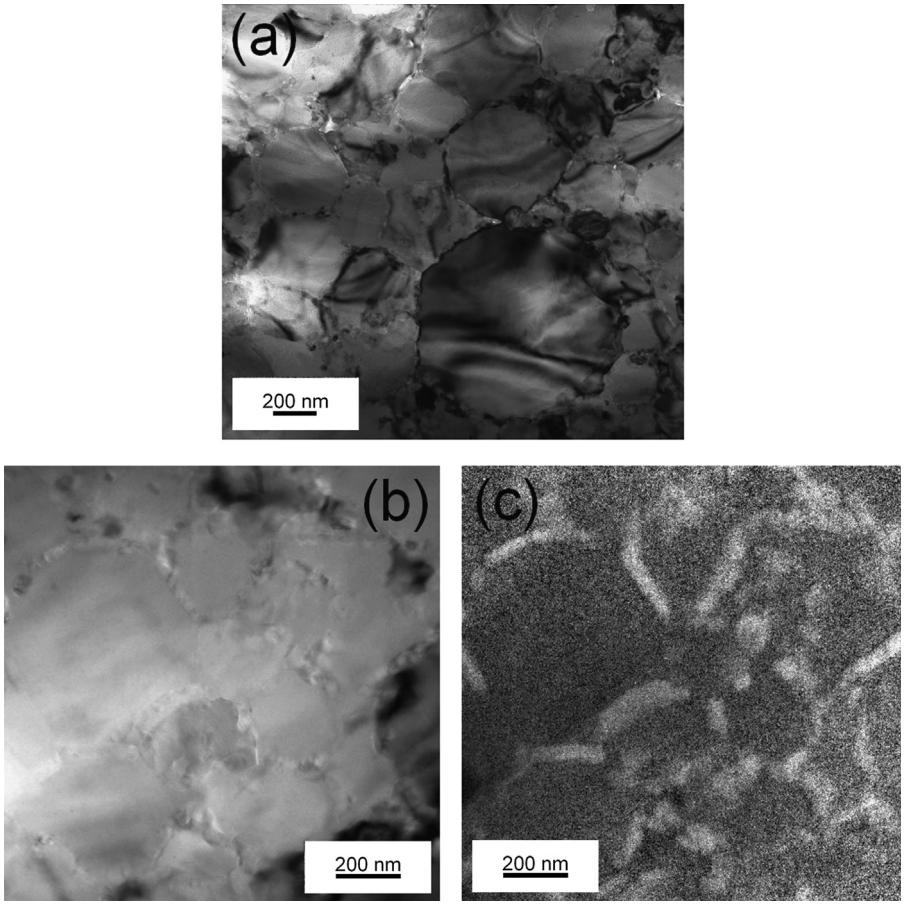

Fig. 2. (a) and (b) Bright-field TEM images for sample UFG-Zn-H. (c) EFTEM image showing the element map for oxygen. The lighter the color in (c) the higher the oxygen content.

containing high and low amounts of oxide phase are referred to as UFG-Zn-H and UFG-Zn-L, respectively.

The grain size values for materials UFG-Zn-H and UFG-Zn-L were 220 nm and 210 nm, respectively, as obtained from TEM investigation. As an illustration, Fig. 2a shows a bright field TEM micrograph for sample UFG-Zn-H. The grain size for both consolidated materials is only slightly larger than the powder particle size (150 nm), which can be explained by the hindering effect of ZnO on the grain coarsening during SPS carried out at high homologous temperature ($0.83 \times T_m$). The fraction of the oxide phase was also investigated by EFTEM analysis. As an example, Fig. 2b and c show a bright field TEM micrograph and the corresponding element map for oxygen obtained by EFTEM. It can be seen that the majority of oxide particles can be found in the grain boundaries of the Zn matrix. The ZnO fractions were 0.15 and 0.05 for UFG-Zn-H and UFG-Zn-L, respectively, as determined from the EFTEM images. These values are in good agreement with the intensity ratios of the ZnO and Zn peaks determined by X-ray diffraction.

Fig. 3 shows a part of the X-ray diffraction pattern for material UFG-Zn-H evaluated by the CMWP method. XLPA investigations revealed that the crystallite size was about 200 nm in the as-consolidated state for both materials UFG-Zn-H and UFG-Zn-L which is close to the grain size determined by TEM. This agreement suggests that the grains are not fragmented into smaller coherently scattering domains (e.g., into subgrains). The dislocation density in both the as-consolidated materials was $0.7 \pm 0.1 \times 10^{14}\,\mathrm{m}^{-2}$. The twin boundary frequency was under the detection limit of XLPA, 0.05%, which corresponds to the twin boundary spacing of 600 nm (if the average spacing of lattice planes is taken as 0.3 nm). This value is much larger

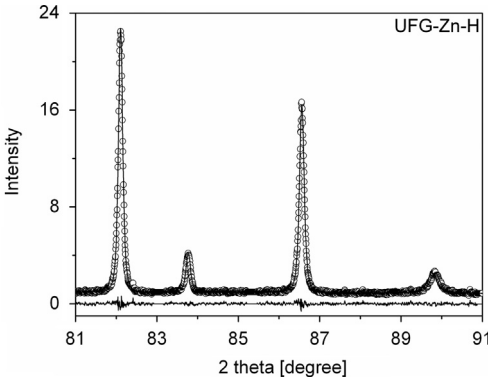

Fig. 3. A part of the X-ray diffraction pattern for the as-consolidated UFG-Zn-H sample evaluated by the CMWP fitting method. The open circles and the solid line represent the measured and the fitted X-ray diffraction patterns, respectively. The difference between the measured and the fitted patterns is also shown at the bottom of the figure.

than the average grain size of ~200 nm in the UFG matrix, which suggests negligible amount of twin boundaries. The lack of twins in UFG-Zn material is in agreement with previous observations which have shown that the probability of twinning in hcp structures decreases with decreasing grain size [18,19], and it has also been confirmed by the present TEM investigations. XLPA study showed that in the as-consolidated state for both materials the fractions of ⟨a⟩- and ⟨c+a⟩-type dislocations were about 60% and 40%, respectively. The abundance of ⟨a⟩-type dislocations can be attributed to their lowest formation energy due to the shortest Burgers vector.

The amount of ⟨c⟩-type dislocation was negligible. These observations are similar to the previous results obtained on other hcp metals [20]. It was also revealed that most of ⟨a⟩- and ⟨c+a⟩-type dislocations were prismatic $(1/3\langle\bar{2}110\rangle\{0\bar{1}\bar{1}0\})$ and pyramidal $(1/3\langle\bar{2}113\rangle\{2\bar{1}\bar{1}2\})$ edge dislocations, respectively.

3.2. High temperature creep behavior

Typical indentation depth–time curves obtained for the material UFG-Zn-H at constant stress and different temperatures are shown in Fig. 4. It is noted that the equivalent stress was set to keep the strain rate between 10^{-5} and 10^{-3} s^{-1}, as the indentation device works well in this range. Therefore, the applied stress for the materials UFG-Zn-H and UFG-Zn-L were in the regimes of 35–55 MPa and 18–30 MPa, respectively. The same strain rate required higher stress in the case of sample UFG-Zn-H due to its larger ZnO content. It is noted that these stresses are about one order of magnitude higher than the values needed for the creep at the same temperature and strain rate regimes in coarse-grained Zn samples [1,2]. Fig. 4 shows that the depth–time curves consist of two stages, corresponding to a short transient and a steady state creep. The slope of the straight line fitted to the steady state regime provided the indentation velocity which was converted into equivalent strain rate using Eq. (2). The strain rate of high-temperature steady state creep can be expressed as [1]:

$$\dot{\varepsilon} = A\sigma^{1/m}\exp\left(-\frac{Q}{kT}\right), \tag{3}$$

where A is a constant, m is the strain rate sensitivity parameter, Q is the activation energy of creep, k is the Boltzmann constant and T is the absolute temperature. At a given temperature, the slope of the straight line fitted to the plot of the logarithm of the stress versus the logarithm of the strain rate gave the strain rate sensitivity parameter, as illustrated for UFG-Zn-H in Fig. 5. The values of m were 0.12 ± 0.02 and 0.14 ± 0.01 for UFG-Zn-H and UFG-Zn-L, respectively, which did not vary significantly with changing the temperature in the range of 330–360 °C. The activation energy was determined from the plot of the logarithm of the strain rate as a function of the reciprocal temperature at constant indentation stress, as illustrated in Fig. 6 for materials UFG-Zn-H and UFG-Zn-L at 38.8 and 25.4 MPa, respectively. The activation energy changed only slightly with varying the applied stress for both materials. The averages of the activation energies obtained at different stresses were 252 ± 25 and 211 ± 19 kJ/mole for specimens UFG-Zn-H and UFG-Zn-L, respectively.

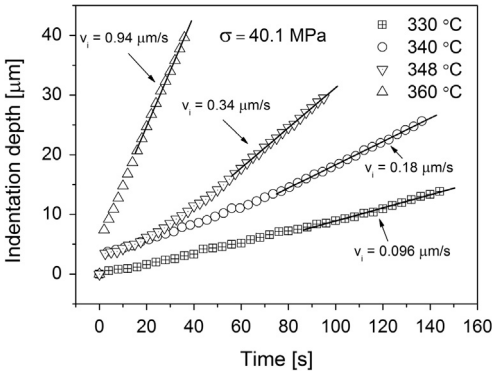

Fig. 4. Indentation creep curves for sample UFG-Zn-H measured at different temperatures. The impression velocity (v_i) was determined as the slope of the linear part of the curves.

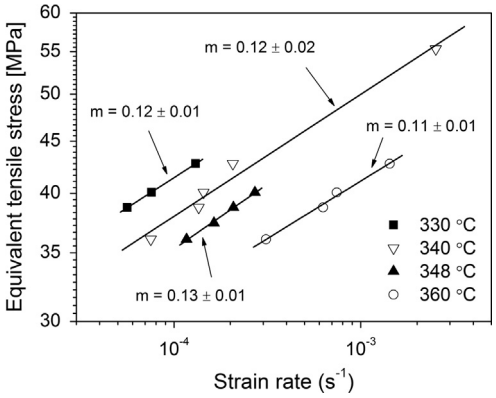

Fig. 5. Equivalent stress vs. strain rate at different temperatures for material UFG-Zn-H. The values of the strain rate sensitivity parameter (m) determined from the slopes of the straight lines are also given in the figure.

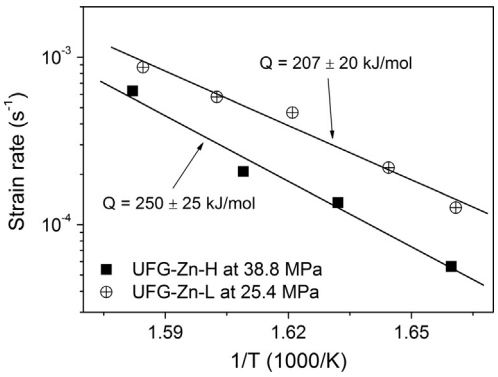

Fig. 6. The logarithm of the strain rate as a function of the reciprocal temperature for materials UFG-Zn-H and UFG-Zn-L at the equivalent stresses of 38.8 and 25.4 MPa, respectively. The slopes of the straight lines give the activation energies of creep for the two samples.

3.3. Microstructure after indentation

In order to reveal the deformation mechanisms occurring during indentation creep, EBSD and XLPA investigations were performed both inside and outside the indented zone after the creep test at 340 °C. Before these measurements the indented surface was mechanically polished first by 1200 grit and then by 2500 grit abrasive papers, thereby removing the material from the surface to the bottom of the indented hole. Then, the samples were polished to a mirror finish by alumina suspension. Finally, the surface layer distorted during mechanical polishing was removed by chemical etching using a mixture of 50% orthophosphoric acid and 50% ethanol. Fig. 7a and b shows EBSD images taken in the indented and non-indented regions, respectively, in material UFG-Zn-H. The grain size was about 250 nm in both regions which is only slightly larger than that in the as-consolidated state. In XLPA experiments the size of the rectangular irradiated area was 0.2 mm × 1.0 mm, which was smaller than the lateral dimension of the indented zone. Therefore, the defect structure could be investigated inside and outside the indented volume separately by X-rays. XLPA showed that the crystallite size and the dislocation density both inside and outside the indented zone agreed within the experimental error with the values determined for the as-consolidated material. Similar results were obtained for material UFG-Zn-L. The unchanged parameters of the microstructure suggest that recrystallization did not occur during creep, despite the long duration (~30 min) and the high homologous temperature (0.88) of this process. The good thermal stability of the UFG-Zn samples can be attributed to the presence of oxide particles which hinder recrystallization. Fig. 7c shows two peaks in the misorientation angle distributions at about 67°

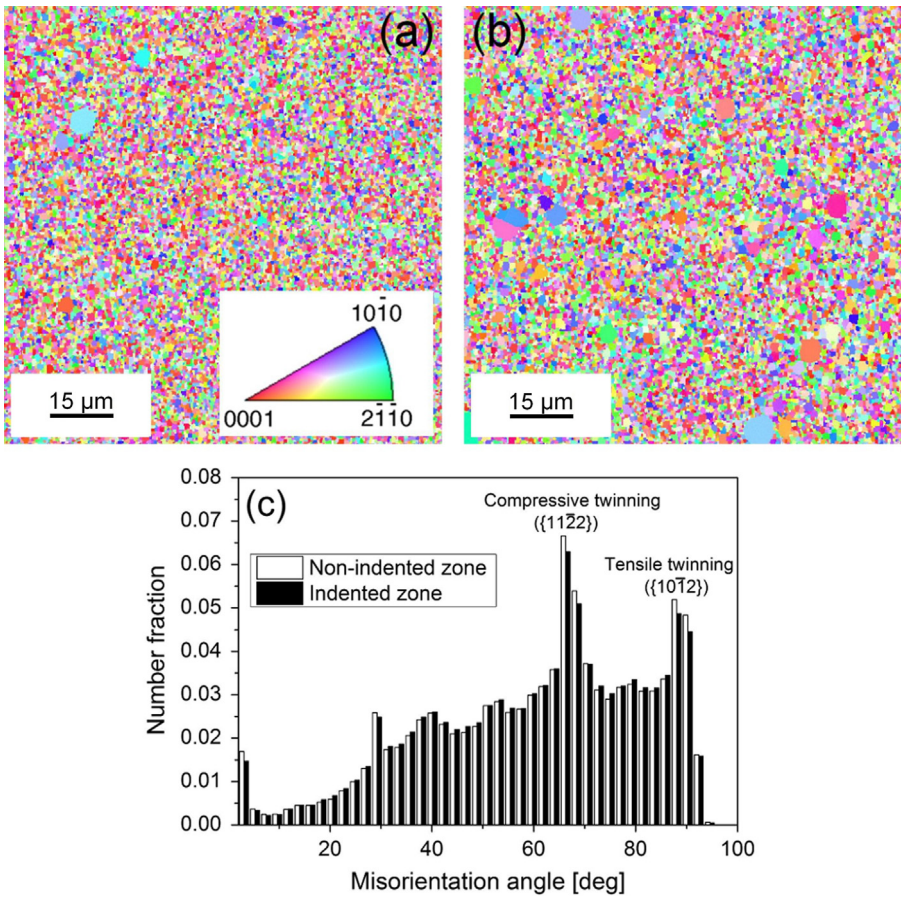

Fig. 7. EBSD images showing the morphology of the grains (a) inside and (b) outside the zone indented at 340 °C. The color code of the standard stereographic triangle inset in (a) illustrates the grain orientations. The misorientation angle distributions determined inside and outside the indented region are shown in (c).

and 90° which correspond to $\{11\bar{2}2\}$ compressive and $\{10\bar{1}2\}$ tensile twins, respectively. At the same time, the twin boundary frequency determined by XLPA remained negligible in both the indented and non-indented zones of the samples. This indicates that the twin boundary frequency in UFG-Zn is under the detection limit of XLPA, as discussed above.

XLPA revealed a difference between the populations of the dislocation slip systems inside and outside the indented zone for both UFG-Zn specimens. In the non-indented volumes the types and fractions of ⟨a⟩- and ⟨c+a⟩-type dislocations were the same as in the as-consolidated state (60% ⟨a⟩-type $1/3\langle\bar{2}110\rangle\{0\bar{1}\bar{1}0\}$ prismatic and 40% ⟨c+a⟩-type $1/3\langle\bar{2}113\rangle\{2\bar{1}\bar{1}2\}$ pyramidal dislocations). At the same time, in the indented zone besides these slip systems significant amount of ⟨a⟩-type $1/3\langle\bar{2}110\rangle\{0001\}$ basal and $1/3\langle\bar{2}110\rangle\{10\bar{1}1\}$ pyramidal dislocations, as well as other ⟨c+a⟩-type $1/3\langle\bar{2}113\rangle\{10\bar{1}1\}$ pyramidal dislocations were detected. The difference between the population of the dislocation slip systems inside and outside the indented zone indicates a considerable dislocation activity during deformation, despite the same value of the dislocation density in the two regions. Additionally, the fractions of ⟨a⟩- and ⟨c+a⟩-type dislocations were slightly higher (71%) and lower (25%), respectively, in the indented zone than outside this region. The amount of ⟨c⟩-type dislocations remained negligible (4%).

4. Discussion

Previous experiments [1–3] on coarse-grained Zn (the grain size is several hundreds of microns) have shown that above $0.5 \times T_m$ two temperature ranges can be distinguished according to the creep behavior. Between 0.5 and $0.6 \times T_m$ the activation energy is close to the self-diffusion activation energy (92 kJ/mole [1]), which suggests that the rate controlling mechanism of the creep is the climb of jogged dislocations occurring via vacancy migration. In the temperature range of $0.8–1.0 \times T_m$ the creep of coarse-grained Zn can be characterized by anomalously high activation energy (152–159 kJ/mole [2,3]). Since a similar large value of Q was obtained for single crystalline Zn oriented for non-basal dislocation glide, the high activation energy is usually explained by thermally activated overcoming of Peierls forces on prismatic and pyramidal slip planes as a rate controlling mechanism. The resistance to shear on non-basal systems decreases strongly with increasing temperature, yielding high temperature sensitivity of creep rate (i.e., activation energy) above $0.8 \times T_m$ [1–3]. In the present experiments performed in the high temperature regime ($0.87–0.91 \times T_m$), the activation energy of the creep for both UFG-Zn samples was also very high (211–252 kJ/mole), suggesting that the rate controlling mechanism is the dislocation glide on non-basal planes. Indeed, considerable twinning was not observed during deformation while a significant fraction of non-basal dislocations was detected even in the as-consolidated materials by XLPA. The activity of dislocations was proved by the change in the population of the different slip systems during creep. Former studies [1,4] have suggested that in coarse-grained Zn dynamic recrystallization also contributes to the anomalously high activation energy of the creep above $0.8 \times T_m$. In the present Zn samples the UFG microstructure remained stable even after long creep experiments due to oxide dispersoids at the grain boundaries. This proves that very high activation energy can be detected in Zn even if recrystallization does not occur.

The activation energy of the creep for both UFG-Zn samples (211–252 kJ/mole) is even larger than the values obtained previously for coarse-grained pure Zn (152–159 kJ/mole) in the same temperature range. The higher activation energy cannot be simply attributed to the smaller grain size in UFG-Zn since our materials contain considerable amount of ZnO which may also have an effect on the activation energy. Oxide-free UFG metallic materials are hard to produce by powder metallurgy, as usually a native oxide layer forms on the surface of the nanosized powder particles during their processing before consolidation. Therefore, in the present study the activation energy of the oxide-free UFG-Zn with the grain size of 200 nm was estimated by a linear extrapolation using the values determined for the samples containing different oxide fractions. The activation energies of 211 ± 19 and 252 ± 25 kJ/mole obtained for the oxide contents of 5% and 15% (as determined by EFTEM analysis), respectively, were extrapolated to zero ZnO fraction which yielded 191 ± 25 kJ/mole for the oxide-free UFG-Zn material. This value is slightly larger than the activation energy for pure coarse-grained Zn (152–159 kJ/mole), suggesting that the lower grain size resulted in higher activation energy of the creep. A similar trend has also been observed for coarse-grained Zn samples when the grain size decreased from 150 to 18 μm [21]. However, in the case of face centered cubic metals the reduction of the grain size into the UFG regime resulted in smaller activation energy of the creep [22], therefore additional experiments on other hcp metals and theoretical considerations are necessary for the explanation of the present result.

The present investigations indicate that the activation energy of the creep in UFG-Zn increases with increasing oxide content. This result is in accordance with previous observations which showed that the activation energy of the creep in dispersion-strengthened metals was higher than that in the pure matrix materials [23–25]. This effect has been successfully explained by both the detachment [23] and jog nucleation [24] models. In the first case there is an attractive interaction between dislocations and dispersions, and the thermally activated detachment of dislocations from dispersoid particles contributes to the activation energy of the creep in addition to dislocation climb. In the second model besides climb the nucleation and separation of a jog pair at the particle-matrix interface is considered to be necessary for particle by-pass by dislocations. Therefore, the creep activation energy in dispersion-strengthened metals exceeds that for volume diffusion. It is noted that the strain rate sensitivity parameter also depends slightly on the ZnO content. Its value decreased from 0.14 ± 0.01 to 0.12 ± 0.01 when the oxide fraction increased from 5% to 15%. Similar observations have been made for other dispersion-strengthened UFG materials [26]. This effect can also be explained by either the detachment or the jog nucleation models [23,25]. The extrapolated strain rate sensitivity parameter to zero ZnO content is 0.15 ± 0.01, which agrees with the value determined previously for a Zn sample with the grain size of 238 nm consolidated from ball-milled powder [6].

5. Conclusions

High temperature creep behavior of UFG-Zn samples with two different oxide contents processed by powder metallurgy was investigated by indentation technique in the temperature range of 330–360 °C. The microstructure before and after the indentation creep test was studied by EBSD and XLPA. The following results were obtained:

(1) The grain size in the as-consolidated samples was about 200 nm, irrespectively of the ZnO content of the material. Recrystallization during high-temperature indentation creep was not observed, indicating an excellent thermal stability of UFG-Zn samples which can be attributed to the retarding effect of ZnO dispersoids on grain growth. The majority of oxide particles were in the grain boundaries of the Zn matrix.

(2) Although the dislocation density was the same inside and outside the indented zone, the distribution of dislocations among the various slip systems was different in the indented and non-indented volumes. Outside the indented region prismatic ⟨a⟩ and pyramidal ⟨c+a⟩ dislocations were observed by XLPA, while in the indented zone additional ⟨a⟩-type basal and pyramidal dislocations as well as other ⟨c+a⟩-type pyramidal dislocations were detected. This observation suggests that there is a considerable dislocation activity during high-temperature creep of UFG-Zn.

(3) The activation energies of the creep were 252 ± 25 and 211 ± 19 kJ/mole for specimens with high and low oxide contents, respectively, which are much larger than the value determined for coarse-grained Zn (152–159 kJ/mole). The higher activation energy for UFG-Zn processed by powder metallurgy can be attributed partly to the effect of ZnO dispersoids. The strain rate sensitivity parameter decreased with increasing oxide content in accordance with the prediction of previous models elaborated for dispersion strengthened metals.

Acknowledgments

This work was supported in part by the Hungarian Scientific Research Fund, OTKA, Grant no. K-109021 and the French-Hungarian bilateral project (PHC Balaton, Hungarian Grant no. TeT_10-1-2011-0737). The authors are obliged to Noémi Szász for TEM sample preparation.

References

[1] H.J. Frost, M.F. Ashby, Deformation Mechanism Maps, Pergamon Press, Oxford, 1982.
[2] W.J.M. Tegart, O.D. Sherby, Philos. Mag. 3 (1958) 1287–1296.
[3] J.E. Flinn, D.E. Munson, Philos. Mag. 10 (1964) 861–870.
[4] D. Solas, C. Tomé, O. Engler, H. Wenk, Acta Mater. 49 (2001) 3791–3801.
[5] G. Dirras, J. Gubicza, H. Couque, A. Ouarem, P. Jenei, Mater. Sci. Eng. A 564 (2013) 273–283.
[6] X. Zhang, H. Wang, R.O. Scattergood, J. Narayan, C.C. Koch, A.V. Sergueeva, A. K. Mukherjee, Acta Mater. 50 (2002) 4823–4830.
[7] H. Conrad, J. Narayan, Acta Mater. 50 (2002) 5067–5078.
[8] K. Zhou, H. Li, J. Pang, Z. Wang, Physica B 406 (2011) 760–765.
[9] D.H. Sastry, Mater. Sci. Eng. A 409 (2005) 67–75.
[10] G.S. Morthy, D.H. Sastry, Phys. Stat. Sol. (a) 70 (1982) 63–71.
[11] J.C.M. Li, Mater. Sci. Eng. A 322 (2002) 23–42.
[12] G. Cseh, J. Bär, H. Gudladt, J. Lendvai, A. Juhász, Mater. Sci. Eng. A 272 (1999) 145–151.
[13] L. Balogh, G. Tichy, T. Ungár, J. Appl. Cryst. 42 (2009) 580–591.
[14] T. Ungár, J. Gubicza, G. Ribárik, A. Borbély, J. Appl. Cryst. 34 (2001) 298–310.
[15] K. Máthis, K. Nyilas, A. Axt, I. Dragomir-Cernatescu, T. Ungár, P. Lukác, Acta Mater. 52 (2004) 2889–2894.
[16] R. Kuzel Jr, P. Klimanek, J. Appl. Cryst. 22 (1989) 299–307.
[17] C. Dragomir, T. Ungár, J. Appl. Cryst. 35 (2002) 556–564.
[18] K.M. Jassby, T. Vreeland, Mater. Sci. Eng. 27 (1977) 1–9.
[19] M.A. Meyers, O. Vöhringer, V.A. Lubarda, Acta Mater. 49 (2001) 4025–4039.
[20] T. Ungár, J. Gubicza, Z. Kristallogr. 222 (2007) 567–579.
[21] R. Kamel, F. Bessa, Br. J. Appl. Phys. 14 (1963) 459–462.
[22] V. Sklenicka, J. Dvorak, P. Kral, Z. Stonawska, M. Svoboda, Mater. Sci. Eng. A 410–411 (2005) 408–412.
[23] J. Rösler, E. Arzt, Acta Metall. Mater 38 (1990) 671–683.
[24] D. Dunand, A. Jansen, Acta Mater. 45 (1997) 4569–4581.
[25] A. Pichler, E. Arzt, Acta Mater. 44 (1996) 2751–2758.
[26] V. Sklenicka, K. Kucharová, M. Pahutová, G. Vidrich, M. Svoboda, H. Ferkel, Mater. Sci. Eng. A 462 (2007) 269–274.